



# Nickel Complexes of Guanidine Functionalized Trisiloxane

Lucia Pricop<sup>1</sup> · Maria Emiliană Fortună<sup>1</sup> · Dumitru Popovici<sup>1</sup> · Mihai Asandulesa<sup>1</sup> · Carmen Racles<sup>1</sup> · Mirela Fernanda Zaltariov<sup>1</sup> · Narcisa Marangoci<sup>1</sup> · Marcela Savin<sup>2</sup> · Valeria Harabagiu<sup>1</sup>

Received: 4 February 2019 / Accepted: 19 April 2019 / Published online: 25 April 2019  
© Springer Science+Business Media, LLC, part of Springer Nature 2019

## Abstract

The present paper presents the preparation and characterization of Ni complex of a guanidine functionalized trisiloxane as a model compound for polysiloxanes supported metal complexes. The structures of the ligand and its Ni complex are elucidated by theoretical calculations using semi-empirical PM6 and DFT methods, and experimentally confirmed by IR, UV, NMR, SEM and EDX. Thus, a 1/1 ligand/Ni complex with a tetragonal structure was established. As proved by ATG and DSC analysis, the Ni complex is stable up to about 170 °C and is characterized by a T<sub>g</sub> value of 25 °C in dry state. Dielectric measurements revealed a conductivity of  $5.6 \times 10^{-7}$  S cm<sup>-1</sup> at 25 °C for the Ni complex, about ten times higher as compared to that of the ligand, due to the reduction of the conduction activation energy induced by the presence of the metal.

**Keywords** Guanidine functionalized trisiloxane · Nickel complex · Structure · Electrical properties

## 1 Introduction

Transition metals complexes play an important role in the performance of molecular materials, having remarkable conducting and magnetic properties with specific applications in material, supramolecular and bio-chemistry [1]. In addition, the metal complexes of N,O-donor ligands can be used as catalysts in organic synthesis or as biological, clinical and analytical reagents [2, 3]. Homogeneous catalysts have high selectivity and mild reaction conditions requirements, while heterogeneous catalysts are more durable and more easily separated from the reaction products. The advantages of both types of catalysts can be combined by using a homogeneous catalyst immobilized onto a polymer [4]. The nickel catalysts are an important class of heterogeneous catalysts because of their extensive applications, like partial

oxidation, metalation processes and steam reforming [5]. Guanidines are superbases presenting interest as reagents and catalysts in inorganic/polymer chemistry [6, 7]. Many years ago, they were found to be efficient ligands for transition metals in several oxidation states [8], thus being suitable reagents for bioinorganic chemistry and as polymerization catalysts [9]. Tetramethylguanidine was covalently linked to silica and used as supported catalyst for epoxidation and condensation [10, 11], addition [12] and transesterification reactions [13]. pH responsive silica for drug delivery was also prepared by physical attachment of guanidine functionalized polymers to surfaces of the inorganic particles [14]. Guanidine functionalized silica materials were tested as ophthalmic devices [15] or for chemical and biological sensors [16]. Polysiloxanes with their hybrid organic (substituents linked to silicon atoms)—inorganic (Si–O backbone) structure possess a set of rather unusual properties, such as high hydrophobicity, chemical resistance (to oxygen, UV irradiation), a low value of the glass transition temperature (T<sub>g</sub> = –123 °C), and a high decomposition temperature (around 380 °C for polydimethylsiloxane). Moreover, these polymers present a low variation of their physico-chemical characteristics with the temperature [17]. Siloxanes ligands such as polycarboxylates, polyazomethines, polysiloxaneamines or polysiloxanes-glycinate were already shown to have a high affinity for divalent metal ions such Mn<sup>2+</sup>, Ni<sup>2+</sup>, Cu<sup>2+</sup>, Co<sup>2+</sup> or Zn<sup>2+</sup> [18–21]. The aim of the present study

**Electronic supplementary material** The online version of this article (<https://doi.org/10.1007/s10904-019-01161-9>) contains supplementary material, which is available to authorized users.

✉ Maria Emiliană Fortună  
fortuna.maria@icmpp.ro

<sup>1</sup> Department of Inorganic Polymers, “Petru Poni” Institute of Macromolecular Chemistry, 41A Grigore Ghica Voda Alley, 700487 Iasi, Romania

<sup>2</sup> “Antibiotice” SA, 1Valea Lupului Alley, 707410 Iasi, Romania

is to demonstrate the feasibility of guanidine functionalized polysiloxanes supported nickel complexes. To define their structure, a low molecular weight model compound was obtained by reacting a monoglycidopropyl-functionalized trisiloxane with tetramethylguanidine. It was used further as newly synthesized ligand for Ni coordination. A deep characterization of its structure/morphology and physicochemical properties of the complex by means of NMR, IR and UV–Vis spectroscopy as well as by differential scanning calorimetry (DSC), thermogravimetric analysis (TGA), scanning electron microscopy (SEM) coupled with energy-dispersive X-ray spectroscopy (EDX) analysis and dielectric measurements is reported.

## 2 Experimental

### 2.1 Materials

1,1,1,3,5,5,5-Heptamethyltrisiloxane 97% (TS), allylglycidylether 99% (AGE), Karstedt catalyst, 1,1,3,3-tetramethylguanidine 99% (TMGu), Nickel(II) acetate tetrahydrate, and *n*-hexane were purchased from Aldrich and used as received. Toluene (Aldrich) was dried over sodium wire and distilled before using.

### 2.2 Methods

Infrared spectra (FT-IR) were obtained by using a Nicolet 60 SX FT-IR under dry air, at room temperature, on KBr pellets, in the range of 4000–400  $\text{cm}^{-1}$ .  $^1\text{H-NMR}$  and  $^{13}\text{C-NMR}$  spectra were recorded on a Bruker Advance III 400 spectrometer in  $\text{CDCl}_3$ . The presence and ratio of metal and Si were evidenced using an Energy-Dispersive X-ray Fluorescence (EDXRF) system EX-2600 X-Calibur SDD. UV–Vis measurements were performed on a Shimadzu UV-1700 Pharma Spec spectrophotometer. Thermogravimetric data (TGA) were registered on a STA 449F1 Jupiter equipment (Netzsch, Germany), in the temperature range of 30–700  $^\circ\text{C}$ , under nitrogen or air flow (50  $\text{mL min}^{-1}$ ) with a heating rate of 10  $^\circ\text{C min}^{-1}$ . Differential scanning calorimetry (DSC) measurements were conducted on a DSC 200 F3 Maia device (Netzsch, Germany) at heating and cooling rates of 10  $^\circ\text{C min}^{-1}$ , under nitrogen atmosphere, at a flow rate of 50  $\text{mL min}^{-1}$ . A Quanta 200 scanning electron microscope provided with EDX elemental analysis system (Ametek, USA) was used to identify the surface morphology and composition. The dielectric spectroscopy analysis was carried out with a Novocontrol CONCEPT 40 dielectric spectrometer (GmbH Germany), in wide range of frequency (1–10<sup>6</sup> Hz) and temperature (–150 ÷ 80  $^\circ\text{C}$ ). The spectrometer is equipped with the Alpha-A high performance frequency analyzer and the ramp of temperature is developed by a Quatro Cryosystem device with 0.1  $^\circ\text{C}$  stability. The measurements

were performed in dry nitrogen atmosphere avoiding water absorption. The samples were used as pellets sandwiched between two gold coated plate electrodes.

### 2.3 Synthesis of 1,1,1,3,5,5,5-Heptamethyl-3-glycidopropyl-trisiloxane (TS-gp)

TS-gp was prepared by the hydrosilation of AGE with TS ( $\text{Si-H/AGE} = 1/1.03$  molar ratio), in the presence of Karstedt catalyst (1  $\text{mL mol}^{-1}$  Si-H), according to a procedure previously described [16]. The reaction was conducted in toluene (50% w/w) for 6 h at 70–80  $^\circ\text{C}$ . The hydrosilation product was separated by vacuum distillation of the solvent and AGE excess, and was purified by dissolution in *n*-hexane, filtration and vacuum evaporation of *n*-hexane. Yield, 99%.

$^1\text{H-NMR}$  ( $\text{CDCl}_3$ ), ppm:  $\delta = 0.01$  (Si- $\text{CH}_3$ ); 0.5–0.7 (Si- $\text{CH}_2$ ); 1.3–1.7 ( $\text{CH}_2\text{CH}_2\text{CH}_2$ ); 2.6–2.8 ( $\text{CH}_2$  of epoxy cycle); 3.15 (C-H of epoxy cycle); 3.4–3.7 ( $\text{CH}_2\text{-O}$ ).

### 2.4 Synthesis of Guanidine Functionalized Trisiloxane (TS-Gu)

In a typical procedure, 5.5 mmol of TS-gp were mixed with an excess of 1,1,3,3-tetramethylguanidine (TMGu) (5.9 mmol) in 45 mL toluene. The mixture was refluxed for 36 h followed by solvent and TMGu excess removal under reduced pressure to give TS-Gu oily product (88%).

$^1\text{H-NMR}$  ( $\text{CDCl}_3$ ), ppm:  $\delta = 0.01\text{--}0.09$  (Si- $\text{CH}_3$ ); 0.43–0.49 (Si- $\text{CH}_2$ ); 1.26–1.31 ( $\text{CH}_2\text{CH}_2\text{CH}_2$ ); 3.39–3.58 ( $\text{CH}_2\text{-O}$ ); 2.73 and 3.81–3.87 ( $\text{CH}_2\text{-N=}$ ); 2.90 [ $\text{-N}(\text{CH}_3)_2$ ]; 4.70 (CH-OH); (Fig. 3).

$^{13}\text{C-RMN}$  ( $\text{CDCl}_3$ ):  $\delta = 1.74$  ppm (Si- $\text{CH}_3$ ); 13.38 ppm (Si- $\text{CH}_2$ ); 23.06 ppm ( $\text{CH}_2\text{CH}_2\text{CH}_2$ ); 72.46–74.16 ppm ( $\text{CH}_2\text{-O}$ ); 55.34 ppm (CH-OH); 39.17 ppm ( $\text{-CH}_2\text{-N=}$ ); 37.54 ppm [ $\text{-N}(\text{CH}_3)_2$ ]; 162.17 ppm ( $\text{-N=C}$ ); (Fig. 4).

### 2.5 Synthesis of Nickel Complex of Guanidine Functionalized Trisiloxane (TS-GuNi)

TS-Gu (1.0917 mmol) in  $\text{C}_2\text{H}_5\text{OH}$  (10 mL) was stirred at room temperature until complete dissolution and then an excess of  $\text{Ni}(\text{CH}_3\text{COO})_2 \times 4\text{H}_2\text{O}$  (2.1556 mmol) was added. After 2 h of stirring the alcohol was slowly evaporated from the resulted green solution at room temperature. The green solid was washed with water to remove any excess of nickel acetate, then quickly with acetone and dried at room temperature under vacuum. Yield, 95%.

### 3 Results and Discussion

#### 3.1 Synthesis and Structural Characterization of Guanidine Functionalized Trisiloxane (TS-Gu) and of Its Nickel Complex (TS-GuNi)

A new guanidine functionalized trisiloxane (TS-Gu) was prepared by a two-step procedure as depicted in Fig. 1. The TS-Gu was subsequently used as a model ligand in reaction with nickel(II) acetate tetrahydrate, to afford the TS-GuNi complex.

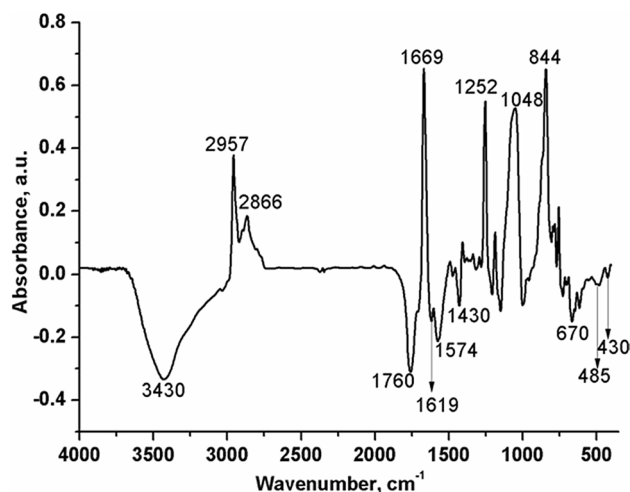
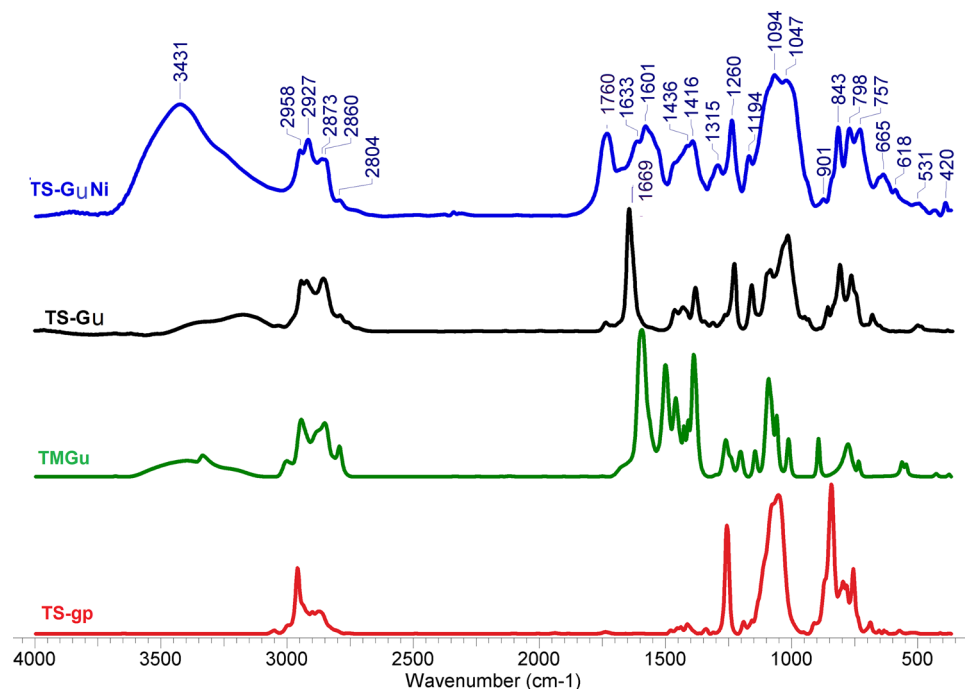


Fig. 1 Synthetic route for the preparation of TS-Gu

Fig. 2 FT-IR spectra of TS-gp, TMGu, TS-Gu and TS-GuNi



Thus, 1,1,1,3,5,5,5-heptamethyltrisiloxane (TS) was first hydrosilated with allyglycidyl ether (AGE) in the presence of a platinum catalyst, according to a procedure previously described [17, 22]. In a second step, the resulted glycidoxypropyltrisiloxane (TS-gp) was reacted with tetramethylguanidine (TMGu) to obtain the guanidine functionalized trisiloxane (TS-Gu). Similar procedures were used to functionalize silica particles with guanidine superbases [10, 23].

The hydrosilation was monitored by evaluating the disappearance of the Si–H characteristic absorption band at  $2160\text{ cm}^{-1}$  in FTIR spectrum of the reaction mixture, band that is not any more visible in the spectrum of the purified TS-gp product (Fig. 2).

The second step was followed by the disappearance of =NH (TMGu) and oxirane (TS-gp) characteristic bands at  $3335$  and  $3050\text{ cm}^{-1}$ , respectively, in the FTIR spectrum of TMGu/TS-gp reaction mixture, proving the completion of the addition of TMGu to the epoxy ring of TS-gp. After purification, the FTIR spectrum of the resulted guanidine functionalized trisiloxane (TS-Gu) (Fig. 2) presents characteristic bands for both trisiloxane (asymmetric Si–O–Si stretching vibration overlapped with C–O–C vibration at  $1100\text{--}1000\text{ cm}^{-1}$ , symmetric deformation/rocking vibrations of the Si–CH<sub>3</sub> group at  $1258\text{ cm}^{-1}$  and Si–CH<sub>3</sub> stretching vibration at  $843\text{ cm}^{-1}$ ). The amidine C=NH strong band at  $1597\text{ cm}^{-1}$  in the spectrum of TMGu moved after reaction with TS-gp and the formation of azomethine band (C–N=C) at  $1669\text{ cm}^{-1}$ .

The structure of TS-Gu was confirmed by proton and carbon NMR spectra (Fig. 3). Thus, following the epoxy ring opening, its proton signals—two peaks of CH<sub>2</sub> and

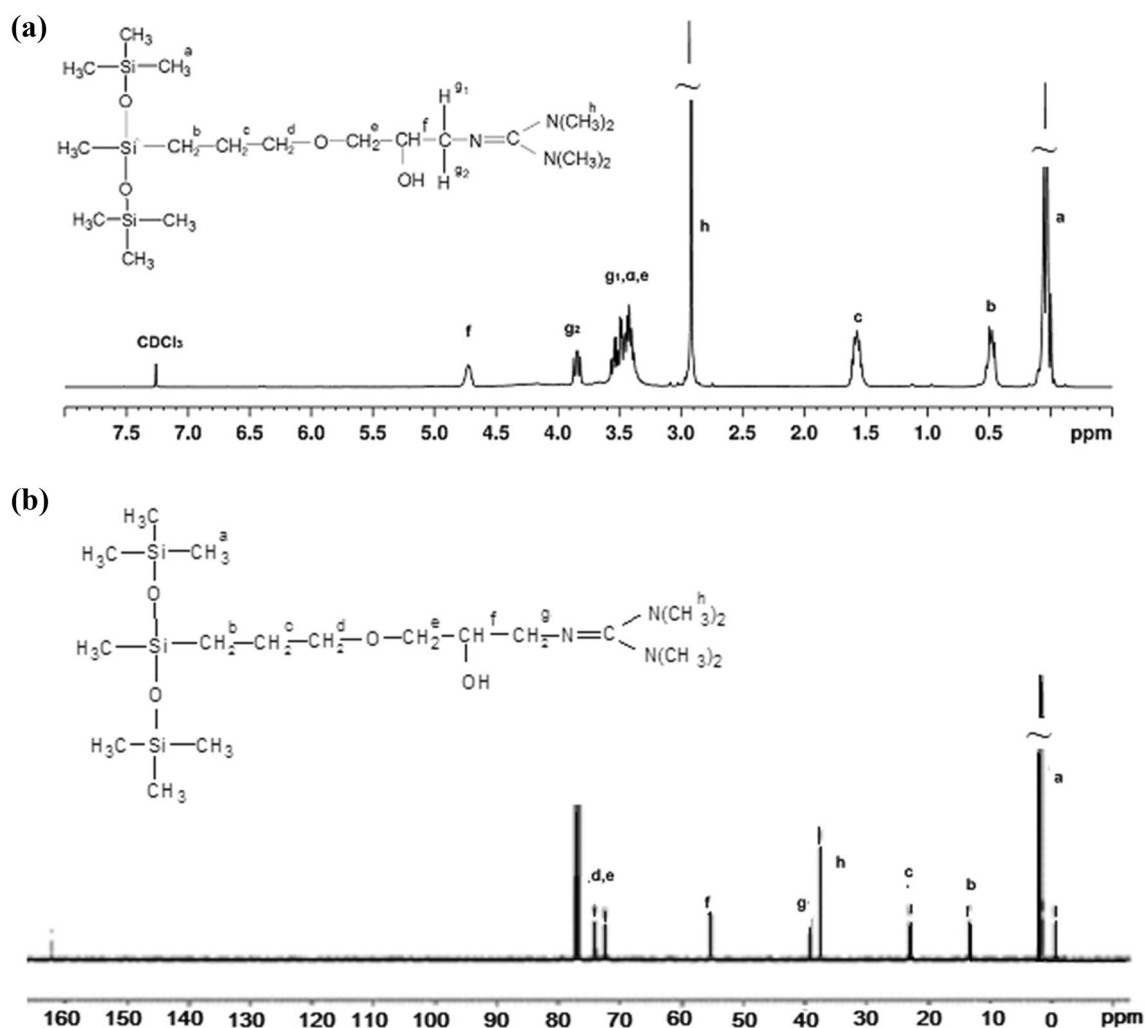


**Fig. 3** <sup>1</sup>H (a) and <sup>13</sup>C-NMR (b) spectra of TS-Gu

one multiplet of CH protons of TS-gp (centered at 2.66, 2.79 ppm and at 3.14 ppm, respectively; see Experimental Section) changed their splitting and moved to 3.51, 3.78 and, respectively, to 4.64 ppm in the spectrum of TS-Gu (Fig. 3a). The peak of HN= protons at 4.76 ppm characteristic for TMGu disappeared and a new peak at 4.64 ppm, characteristic to CH–OH protons appeared, while the resonance peak of methyl protons visible at 2.68 ppm in the spectrum of TMGu moved at 2.85 ppm in the spectrum of TS-Gu. Moreover, the integral ratios of the characteristic proton signals correspond to the proposed structure.

<sup>13</sup>C-NMR spectrum of TS-Gu also proved the proposed structure by the presence of the specific signals for the formed product (55.34 ppm for CH–OH and 162.17 ppm for –N=C) (Fig. 3b).

The coordination of nickel acetate to TS-Gu was performed at room temperature by stirring the reagents in ethanol solution. The Ni(II) complex (Fig. 4), was isolated as a greenish amorphous solid.

Unfortunately, any attempt to obtain a crystalline morphology was unsuccessful due to the large and flexible structure of the trisiloxane ligand. Thus, the structure of TS-GuNi product was first analyzed by IR spectroscopy (Fig. 2). The main differences between the spectra of TS-Gu and of Ni(II) complex were highlighted by using the method of IR spectral subtraction with Bruker OPUS 6.5 software (see Fig. 1 and comment, Supporting Information). Based on the magnitude of the separation between asymmetric and symmetric carboxylate stretching [24–26], a bidentate chelating mode of the acetate group in the Ni(II) complex was established, while the red shifting of C=N band by about 90 cm<sup>-1</sup> from 1669 to 1760 cm<sup>-1</sup> in the spectrum of TS-GuNi(II) complex proves that minimum nitrogen atom [(CH<sub>3</sub>)<sub>2</sub>N]<sub>2</sub>C=N<sup>+</sup>H is involved in the coordination on Ni<sup>2+</sup> [27].

The composition of the Ni complex (TS-GuNi) is closed, in the limit of the experimental errors, to those theoretically calculated for a 1/1 complex, as proved by EDX analysis (see Fig. 2, Supporting Information).

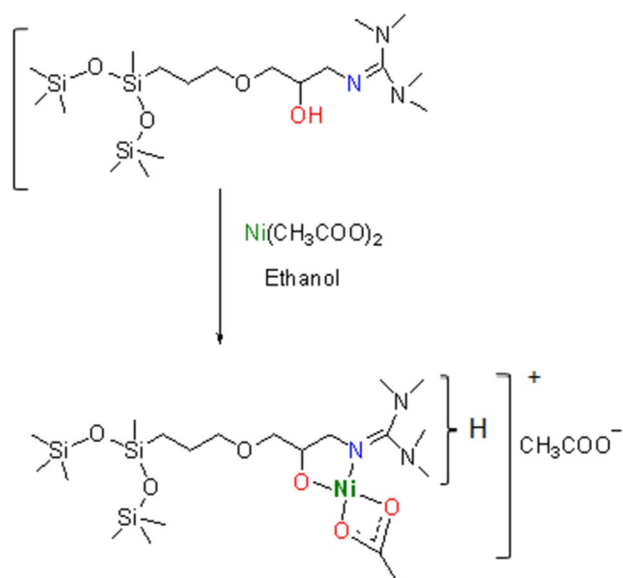


Fig. 4 The reaction pathway to obtain the Ni(II) complex

### 3.2 Theoretical Study of the Conformation of Organometallic Complexes

To elucidate the structure of TS-GuNi complex, quantum calculations were performed for TS-Gu ligand (formally named L) and for two of the possible structures of its Ni complex, namely L1-Ni and L2-Ni containing one, respectively, two ligand molecules linked to the Ni atom (Fig. 5).

The minimum conformation energies for all these structures were obtained in two steps. In the first step, semi-empirical PM6 method implemented in MOPAC2016 was used [28]. A pKa value of 16.1, close to the experimentally determined one of 15.2 [14] was calculated with this method for TS-Gu, denoting the well-known very strong basic character. A second minimization step was conducted using DFT method at B3LYP/6-31G(d,p) [29, 30] level of the theory implemented in GAMESS-US software under Linux as operation system [31]. 3D conformations at minimum energy for the ligand and for the proposed structures of the complexes are also presented in Fig. 5 (grey—C, blue—N, red—O, metallic grey—Si, light grey—H, green—Ni). The Hessian and implicitly the vibrational frequency spectrum were calculated for each of these structures at minimum energy using the same level of the quantum theory. According to the literature, for low frequency ( $\nu < 2000 \text{ cm}^{-1}$ ), a correlation factor of 0.9627 has been applied, with an overall root-mean-square error,  $\text{rms}\nu = 33 \text{ cm}^{-1}$  determined for this correction [32]. By comparing the calculated spectra of the complex structures with the experimental one obtained for TS-GuNi the best correlation is observed for L1-Ni structure (see Fig. 3, Supporting Information).

The experimental and calculated characteristic frequencies for TS-GuNi and L1-Ni, respectively are presented in Table 1.

Disrupted bonding and anti-bonding orbitals were calculated for L1-Ni and L2-Ni structures, while the orbital distributions are extended over the entire molecule, contrary to the ligand structure, were all orbitals are located either on siloxane moiety or on the functional group (see Fig. 4, Supporting Information).

Using TD-DFT method at B3LYP/6-31G(d,p) level of the theory, the UV–VIS spectra have been calculated (Fig. 6). From this figure one may observe an important red shift which can be attributed to a substantial decrease of the band gap for the proposed structures of the Ni complex in the excited state (1.32 eV for L1-Ni and 1.21 eV for L2-Ni) as compared to that corresponding to the ligand of 4.93 eV. Thus, transitions that include those characteristics for low energy photons become possible.

The presence of the Ni(II) sites was readily confirmed by UV/VIS spectroscopy in the solid state (Fig. 6d). Comparing calculated UV–VIS spectra with the experimental one and the absorption peak values in Table 2, the best correlation was observed for L1-Ni structure, similar to the results obtained by FTIR analysis.

All these data confirm that L1-Ni structure is the best candidate for a real structure of the obtained TS-GuNi complex. However, the possible formation of the L2-Ni structure could not be entirely excluded, as the elemental analysis by XPS gave a Si/Ni atomic ratio of 3/1.2.

Based on B3LYP/6-31G(d,p) calculation, the interatomic distances and the bond angles for L1 and L1-Ni are presented in Table 3. As one may see from the data in Table 3, both structures are twisted due to the steric hindrance of the substituents linked to the guanidine structure [33].  $\rho$  values of 0.91 and 0.96 were calculated for L1 and L1-Ni structures, respectively, with the relation  $\rho = \text{length}_{\text{C14=N1}} / (\text{length}_{\text{C14=N2}} + \text{length}_{\text{C14=N3}})$  [34], as measures of the degree of electron delocalisation within guanidine moiety. Similar values were obtained for free guanidine ligands [35] and for guanidine-metal complexes [33], the higher values for complexes being a result of the metal charge stabilisation. The adopted symmetry of metal ion is plan-square, but a slight deviation from flatness has been noticed (Fig. 7). Moreover, the TS-GuNi complex (Fig. 6d) shows an absorption band at around  $14,000 \text{ cm}^{-1}$  with a multiplet structure similar to that of other Ni(II) complex with a siloxane-based linker [36].

In agreement to the Tanabe–Sugano diagram, the most probable electronic transitions are the spin-allowed  ${}^3T_{1g}(\text{F}) \rightarrow {}^3T_{1g}(\text{P}) (\nu_3)$ , characteristic to a tetrahedral environment around the Ni(II) ion [37].



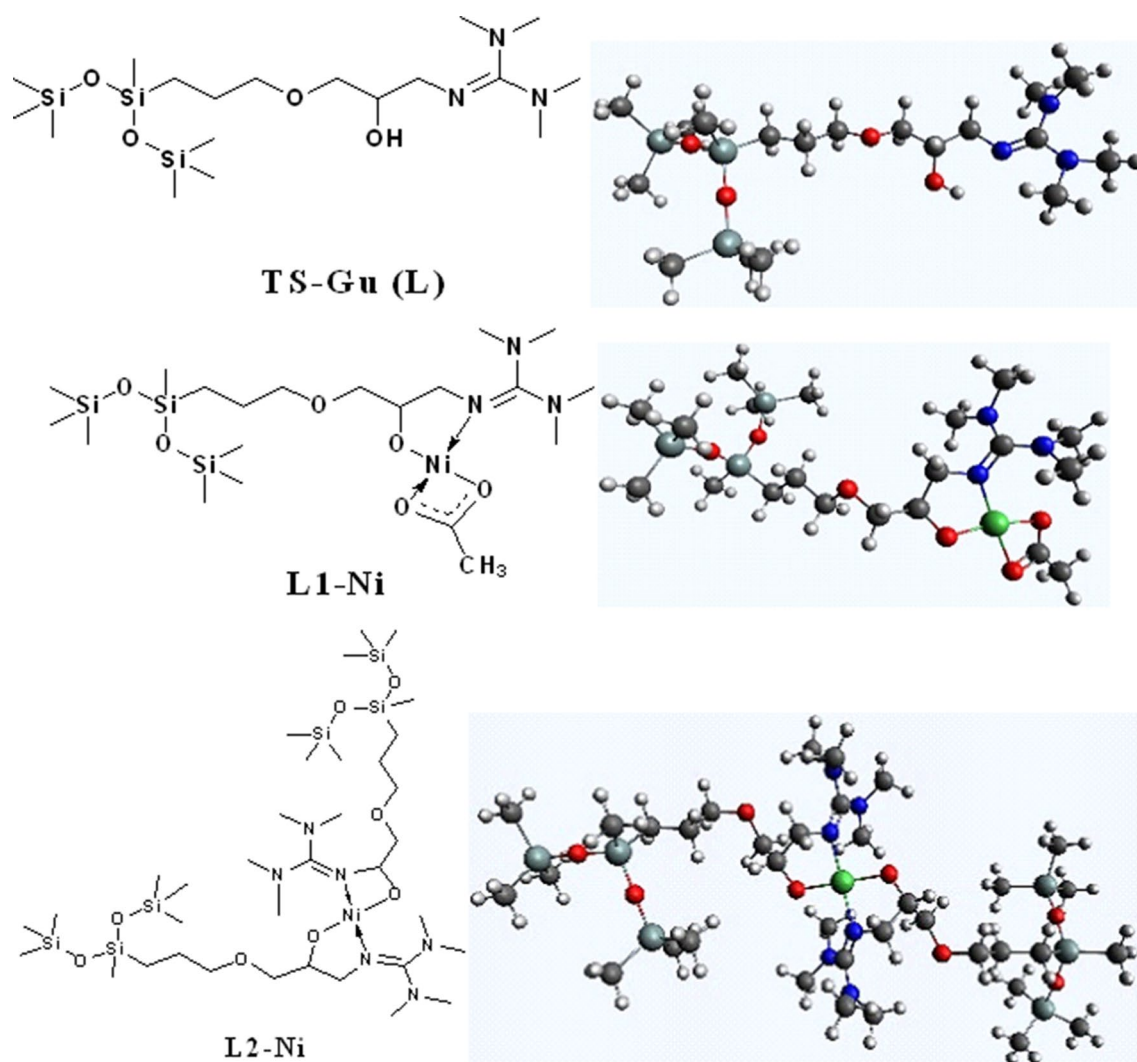


**Fig. 5** Chemical structure of the TS-Gu ligand and of the proposed structures of its complexes (Color figure online)

### 3.3 Thermal Properties of the TS-Gu Ligand and the Metal Complex

The thermal decomposition of the TS-Gu ligand and of TS-GuNi complex was studied by thermogravimetric analysis under nitrogen flow (Fig. 8). TS-Gu decomposes in four steps with maximum decomposition peaks situated at about 152, 262, 366 and 403 °C (Fig. 8a). At temperatures higher than about 410–700 °C, no decomposition phenomena were observed, the residual mass being of 13.96%. For TS-GuNi complex, a similar four step decomposition behaviour was registered, but the maximum decomposition peaks are situated at different temperatures, at about 84, 199, 309 and 406 °C (Fig. 8b). Combined FTIR and MS analysis of the evolved gases (not shown) indicated that the first decomposition step is concerned with water loss.

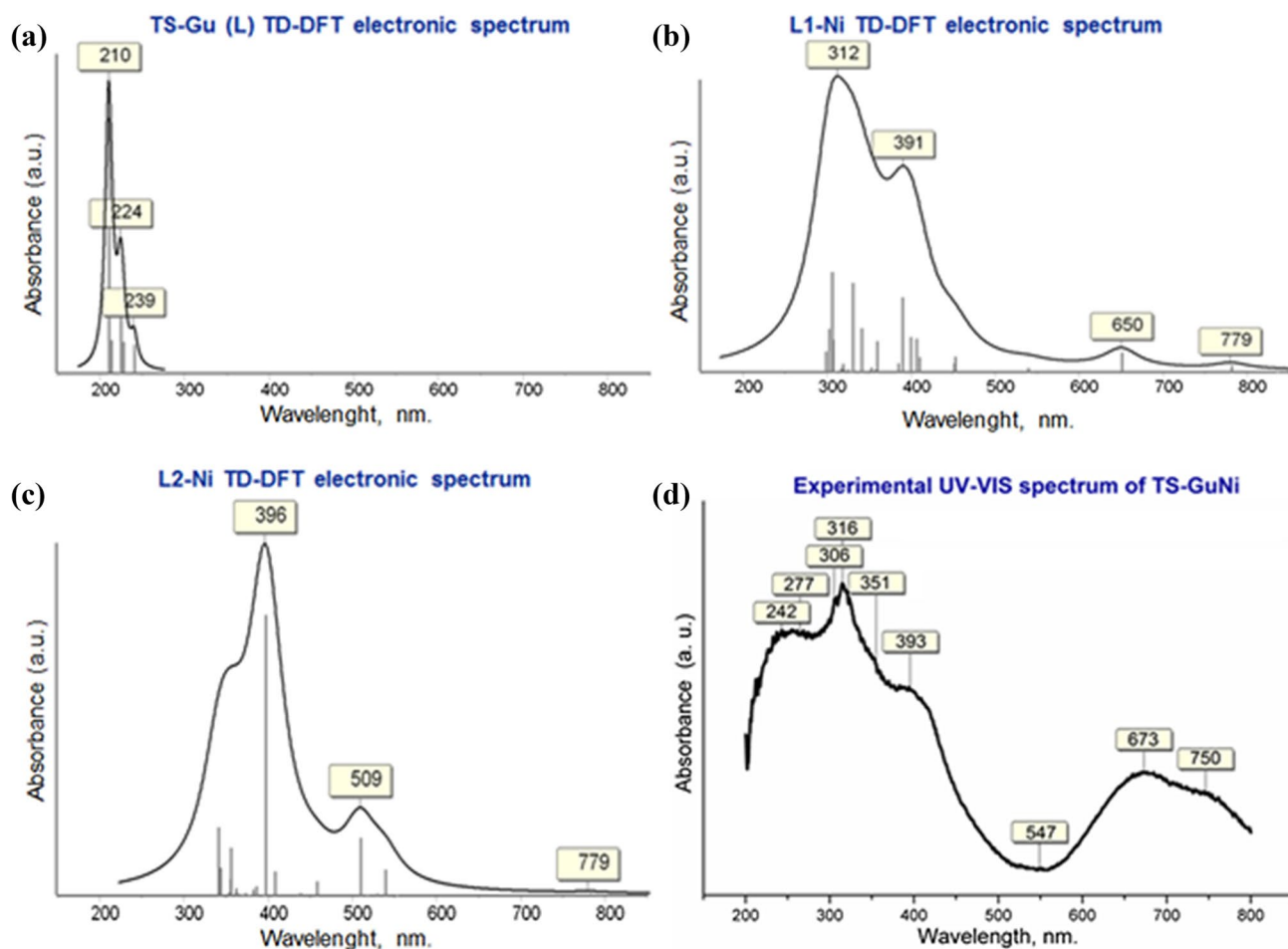
According to TG data, TS-GuNi is thermally stable up to about 171 °C when its decomposition practically starts. The next three steps are related to the decomposition of the ligand. At temperatures higher than about 510–700 °C, no decomposition phenomena were practically observed, the residual mass being of 45%.

The calculated value of residual metals in the form of oxides for TS-GuNi structure having Ni atom coordinated to one ligand molecule is 35.32%. When the decomposition process was carried out in air (not shown), similar decomposition behaviour was evidenced and a residual mass of 34.08% was obtained, very closed to the calculated value, confirming the TS-Gu/Ni ratio of 1/1.

The DSC analysis for TS-Gu ligand and of its TS-GuNi complex was made between – 150 and 150 °C (see Fig. 5, Supporting Information).

**Table 1** Absorption frequencies experimentally observed for TS-GuNi and calculated for L1-Ni

Experimental (cm <sup>-1</sup> )	Calculated (cm <sup>-1</sup> )	Assignment (according to Reference [17])
420	414	N → Ni bending
465	473	O → Ni ← N sym stretching
525	507–532	O → Ni ← N asym stretching
618	633	O–Ni ← N asym stretching
665		Guanidine deformation
757, 798, 843, 718	775–910	Si–C stretching (Si–CH <sub>3</sub> )
901		C–O–C sym stretching
1094	1099	Si–O–Si asym stretching
1194	1170–1197	C–N stretching (tertiary C–N)
1260, 1315	1280–1352	CH <sub>3</sub> umbrella mode and CH <sub>2</sub> wagging (Si–CH <sub>3</sub> )
1416		O–CH <sub>2</sub> (CH <sub>2</sub> scissoring)
1436	1436–1550	Methyl and methylene vibration
	1518	CH <sub>3</sub> –COO stretching
	1596	COO carboxyl asym stretching
1601, 1653	1579, 1644	C=N stretching (guanidine)
1752		C=N, C=O stretching overlapping
2800–2960	2883–3107	CH <sub>3</sub> CH <sub>2</sub> (CH sym and asym stretching)
3431		O–H stretching (H <sub>2</sub> O trace)

**Fig. 6** Calculated UV–VIS spectra for TS-Gu ligand and for the proposed structures of its Ni complex (a–c), and experimental UV–VIS spectrum for TS-GuNi (d)

**Table 2** Calculated UV/VIS absorption peaks for L1-Ni structure and experimentally determined for TS-GuNi complex

Experimental (nm)	Calculated (nm)
306	305
316	312
334	330
351	358
393	391
547	539
673	650
750	779

**Table 3** Calculated inter-atomic distances and angles for TS-Gu ligand (L1) and its L1-Ni complex

Position with respect to the Ni <sup>+2</sup> ion	L1	L1-Ni
C14=N1	1.264	1.313
C14=N2	1.390	1.373
C14=N3	1.394	1.380
N1=C14-N2	119.6	120.6
N1=C14-N3	126.3	123.4
N2-C14-N3	114.0	116.0
N1-N2-N3-C14 (°)	- 0.9	- 0.4
N1 → Ni (Å)	-	1.856
O4-Ni (Å)	-	1.786
O6-Ni (Å)	-	1.937
O5 Ni (Å)	-	1.917
O5 → Ni ← N1 (°)	-	169.3
O4-Ni-O6 (°)	-	165.9
O4-Ni ← N1 (°)	-	88.6
O6-Ni ← N1 (°)	-	102.9
O4-Ni ← O5 (°)	-	99.0
O6-Ni ← O5 (°)	-	68.5

### 3.3.1 Conductivity Behavior

Dielectric spectroscopy is a versatile technique that highlights various physical and chemical properties of a given material. Broadband dielectric measurements coupled with a high quality temperature control system are generally employed to emphasize dipolar relaxation processes in polymers, being a powerful tool for examining the molecular dynamics in polymers and polymer composites [38, 39]. Given the sensitivity of the method, and the expected modification of the dielectric parameters due to the presence of metal centers, the dielectric properties of the metal complex was analyzed in comparison with the ligand, thus further confirming the complexation reaction.

### 3.3.2 Electrical Modulus Analysis

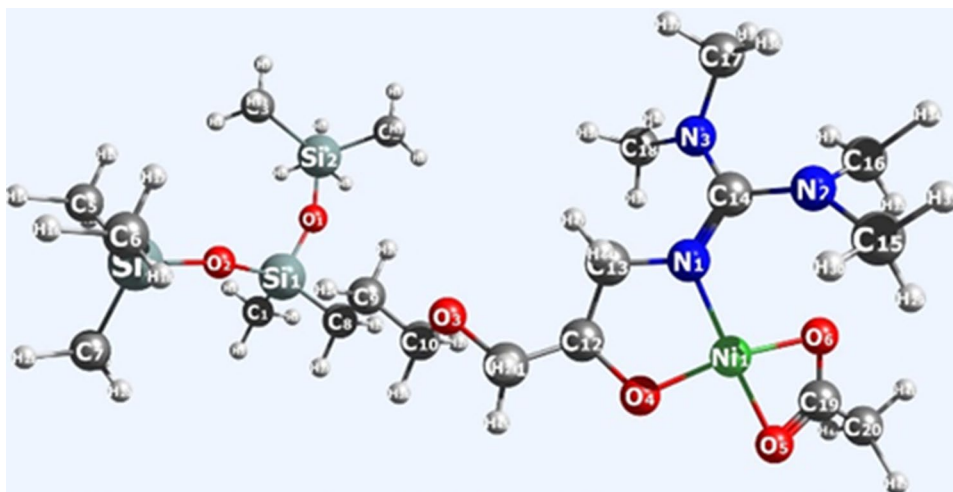
In order to investigate the conductivity of a material, an electrical modulus analysis is necessary. The complex quantity  $M^*$  is expressed by the Eq. (1):

$$M^*(f) = \frac{1}{\epsilon^*(f)} = M' + iM'' \quad (1)$$

where  $M'$  is the real component of the modulus and  $M''$  is the imaginary part.

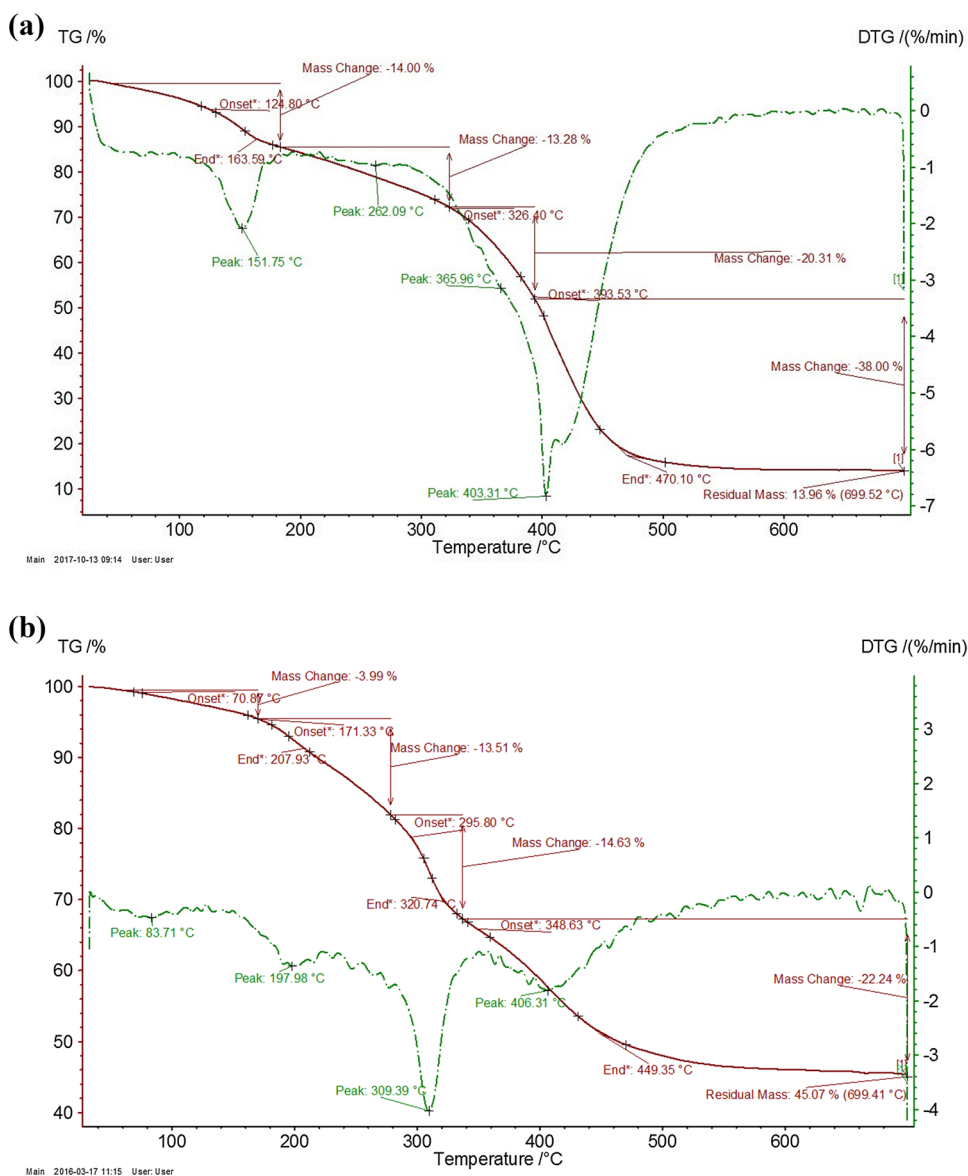
Generally, for polymers, the electrical modulus,  $M^*$ , is widely used to characterize the conductivity process, given the fact that the effect of electrode polarization is suppressed in  $M''$  representation and the dipolar relaxations are better emphasized.

The temperature dependences of  $M''$  for TS-Gu ligand and TS-GuNi complex and the 3d version of  $M''$  versus frequency and temperature where the dipolar relaxations are emphasized are displayed in Fig. 9 and, respectively Fig. 6, Supporting Information.

**Fig. 7** L1-Ni proposed structure with labeled atoms



**Fig. 8** Thermogravimetric curves of TS-Gu (a) and of TS-GuNi (b)



The primary  $\alpha$ -relaxation connected to glass transition is clearly revealed for TS-Gu only at low frequency (1 Hz), while the secondary  $\beta$ -relaxation is observed in the  $M''$  diagram of TS-GuNi. Moreover,  $M''$  evolution of both TS-Gu and TS-GuNi reveals a supplementary dielectric peak, that encloses the primary relaxation connected to the glass transition and is associated with the conductivity process ( $\sigma$ ). The conductivity peak maxima shift gradually to higher temperatures with increased frequencies, suggesting that these processes are thermally activated.

### 3.3.3 AC Conductivity, $\sigma_{AC}$

From  $\sigma$ -frequency dependence as a function of temperature, an about ten times higher conductivity magnitude for the Ni

complex than that for the ligand was determined (see Fig. 7 and comment, Supporting Information).

Figure 10 presents a comparative representation of the conductivity as a function of temperature for both analyzed samples. At low temperatures, the dependences show similar behavior and are almost overlapped for all selected frequencies. At positive temperatures, the magnitude of  $\sigma$  characteristic to the complex (plotted with black) is higher than that of the ligand (plotted with red), indicating a higher conductivity. Supplementary, TS-Gu sample reveals the position of  $\alpha$ -relaxation connected to  $T_g$  in the  $-15$ – $-5$  °C temperature range.

Furthermore, the AC conductivity is governed by the universal power law:

$$\sigma(f) = \sigma_{DC} + Af^n \quad (2)$$

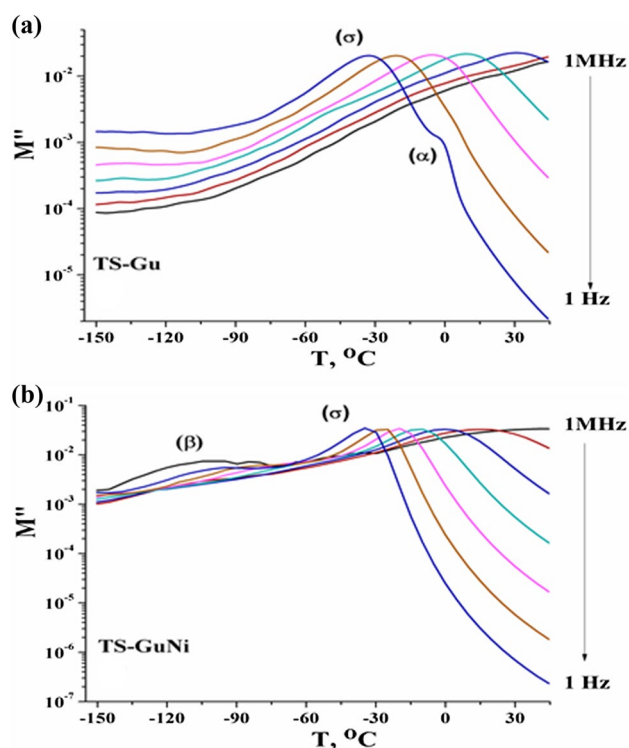


**Fig. 9** Variation of the imaginary component of modulus representation as a function of temperature at selected frequencies for TS-Gu (a) and TS-GuNi (b) samples

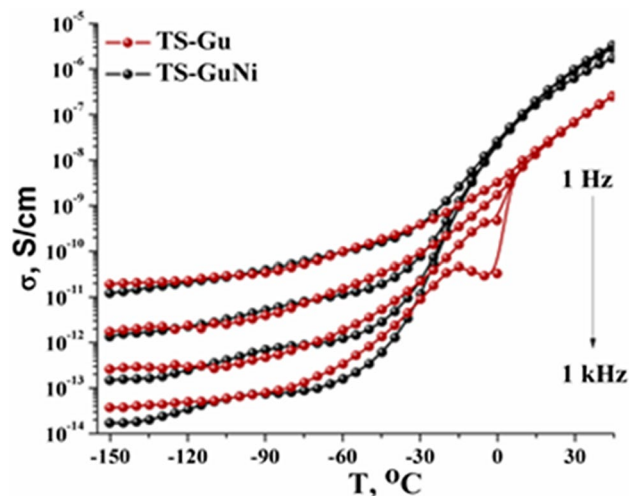


**Fig. 10** Conductivity evolution versus temperature for the TS-Gu and TS-GuNi samples for selected frequencies (Color figure online)

where  $A$  is the pre-exponential factor and  $n$  is the fractional exponent. The exponent gives information about charge transport mechanism and might be calculated from the conductivity dependences versus frequency, plotted in a double logarithmic scale.

Considering the temperature range between  $-150$  and  $-30$  °C,  $n$  varies between 0.8 and 0.4 for TS-Gu ligand and between 1 and 0.3 for TS-GuNi complex (see Fig. 7, Supporting Information). For further increase in temperature,  $n$  considerably decreases up to 0.01 for both samples.

According to literature, this evolution with temperature is characteristic to an electronic conduction via a hopping process [40]. Around  $-10$  °C TS-Gu exhibits a clear and well-distinguished peak assigned to primary  $\alpha$ -relaxation connected to the glass transition.

The values of the thermal activation energy of conductivity were lower than 1 eV, confirming the predominance of the electronic conductivity via a hopping-type mechanism, while activation energy of the metallic complex is lower than for the ligand due to Ni sites that facilitate the charge carrier mobility (see Fig. 9, Supporting Information).

## 4 Conclusion

A new trisiloxane modified with 1,1,3,3-tetramethyl guanidine has been obtained and used as model ligand for polysiloxane supported Ni(II) complexes. The complex structure was determined by comparing experimental data with theoretical calculations.

Broad-band dielectric spectroscopy was used in order to investigate the AC conductivity of the polymer systems.

A ten times higher conductivity magnitude for the organometallic complex than that characteristic to the ligand was found from the conductivity dependences versus frequency. Moreover, from the Arrhenius plots representation of  $\ln \sigma$  versus inverse temperature we concluded that the activation energy of the TS-GuNi complex is lower than  $E_a$  for the ligand due to the presence of Ni sites that facilitates the charge carrier mobility.

The fractional exponent evolution and the conductivity activation energy investigations revealed the predominance of electronic conductivity via a hopping-type mechanism.

**Acknowledgements** The financial support of European Social Fund for Regional Development, Competitiveness Operational Programme Axis 1 under the projects entitled "Petru Poni Institute of Macromolecular Chemistry - Interdisciplinary Pol for Smart Specialization through Research, Innovation and Technology Transfer in Bio(nano) polymeric Materials and (Eco)Technology", InoMatPol, ID P\_36\_570, Contract 142/10.10.2016, cod MySMIS: 107464) and „Novel porous coordination polymers with organic linkers of variable size for gas storage”, POCPOLIG, ID P\_37\_707, MySMIS code 104810, Contract 67/8.09.2016 is gratefully acknowledged.

## References

1. A.M. Reguig, M. Mostafa, L. Larabi, Y. Harek, J. Appl. Sci. **8**, 3191–3198 (2008)

- M.N. Hughes, *The Inorganic Chemistry of Biological Processes*, 2nd ed. (Wiley, Brisbane, 1981) p. 338
- A.Y. Louie, T. Meade, *J. Chem. Rev.* **9**, 2711–2734 (1999)
- L.A. Van de Kuil, D.M. Grove, J.W. Zwikker, L.W. Jenneskens, W. Drenth, G. Van Kotent, *Chem. Mater.* **6**, 1675–1683 (1994)
- J.C. Jesus, I. Gonzalez, A. Quevedo, T. Puerta, *J. Molec. Catal., A: Chem.* **228**, 283–291 (2005)
- D. Margetic, in *Superbases in Organic Chemistry: Guanidines, Amidines, Phosphazenes and Related Organocatalysts*, Chapter 2, ed. by T. Ishikawa (UK, 2009) p. 25.
- Q. Li, T.W. Wang, C. Ma, W. Bai, R. Bai, *A.C.S. Macro. Lett.* **3**, 1161–1164 (2014)
- R. Longhi, R.S. Drago, *Inorg. Chem.* **4**, 11–14 (1965)
- J. Stanek, T. R€osener, A. Metz, J. Mannsperger, A. Hoffmann, S.H. Pawlis, *Top Heterocycl. Chem.* **173** (2015)
- J. Mdoe, *Tanz. J. Sci.* **37**, 156–166 (2011)
- A.C. Blanc, D.J. Macquarrie, S. Valle, G. Renard, C.R. Quinnb, D. Brunela, *Green Chem.* **2**, 283–288 (2000)
- E.J. DeOliveira, D. Torres, C.C. Silva, A.A.M. Luz, P. Bacuzis, A.G.S. Prado, *J. Braz. Chem. Soc.* **17**, 994–999 (2006)
- E.A. Faria, H.F. Ramalho, J.S. Marques, P.A.Z. Suarez, A.G.S. Prado, *Appl. Catal. A: Gen.* **338**, 72–78 (2008)
- A.S. Timin, E.V. Balantsevab, S.Y. Khashirovac, E.V. Rumyantsev, T.Yu. Osadchaya, *Colloids Surf A Physicochem. Eng. Asp.* **477**, 26–34 (2015)
- S. Pinto, P. Alves, C.M. Matos, A.C. Santos, L.R. Rodrigues, J.A. Teixeira, M.H. Gil, *Colloids Surf. B Biointerfaces* **81**, 20–26 (2010)
- G.C. Mackey, in *PhD Thesis*, (Queen’s University Kingston, Ontario, 2016) pp. 108–120.
- V. Harabagiu, M. Pinteala, C. Cotzur, B.C. Simionescu, in *The Polymeric Materials Encyclopedia: Synthesis, Properties and Applications*, vol. 4, ed. by J.C. Salamone, (CRC Press, Boca Raton, 1996), pp. 2661–2667.
- I.M. El-Nahhal, N.M. El-Ashgar, *J. Organomet. Chem.* **692**, 2861–2886 (2007)
- M.F. Zaltariov, M. Cazacu, L. Sacarescu, A. Vlad, G. Novitchi, C. Train, S. Shova, V.B. Arion, *Macromolecules* **49**, 6163–6172 (2016)
- C. Racles, S. Shova, M. Cazacu, D. Timpu, *Polymer* **54**, 6096–6104 (2013)
- M.F. Zaltariov, M. Cazacu, C. Racles, V. Musteata, A. Vlad, A. Airinei, *J. Appl. Polym. Sci.* **132**, 68–246 (2015)
- A.M. Durdureanu-Angheluta, E. Ignat, S.S. Maier, L. Pricop, A. Coroaba, A. Fifere, M. Pinteala, A. Chiriac, *Appl. Surf. Sci.* **292**, 898–905 (2014)
- Y.V. Subba Rao, D.E. De Vos, P.A. Jacobs, *Angew. Chem. Int. Ed. Engl.* **35**, 2661–2663 (1997)
- C. Racles, M.F. Zaltariov, M. Iacob, M. Sillion, M. Avadanei, A. Bargan, *Appl. Catal. B: Environ.* **205**, 78–92 (2017)
- D. Martini, M. Pellei, C. Pettinari, B.W. Skelton, A.H. White, *Inorg. Chim. Acta* **333**, 72–82 (2002)
- V. Zeleňák, Z. Vargová, K. Györy, *Spectrochim. Acta Part A* **66**, 262–272 (2007)
- G. Socrates, *Infrared and Raman Characteristic Group Frequencies. Tables and Charts*, 3rd edition ed. by Socrates, G. (Middlesex, London, 2001), pp. 68–246.
- J.J.P. Stewart, *Comput. Chem.* **10**, 209 (1989)
- H.L. Schmider, A.D. Becke, *J. Chem. Phys.* **108**, 9624–9631 (1998)
- C. Lee, W. Yang, R.G. Parr, *Phys. Rev. B. Condens. Matter.* **37**, 785–789 (1988)
- M.W. Schmidt, K.K. Baldrige, J.A. Boatz, S.T. Elbert, M.S.J. Gordon, H. Jensen, S. Koseki, N. Matsunaga, K.A. Nguyen, S. Su, T.L. Windus, M. Dupuis, *Comput. Chem.* **14**, 1347–1363 (1993)
- J.P. Merrick, D. Moran, L. Radom, *J. Phys. Chem. A.* **111**, 11683–11700 (2007)
- J. Börner, V.I. Santos, M.D. Jones, A. Döring, D. Kuckling, U. Flörke, S. Herres-Pawlis, *Eur. J. Inorg. Chem.* **28**, 4441–4456 (2011)
- V. Raab, K. Harms, J. Sundermeyer, B. Kovacevic, Z.B. Maksic, *J. Org. Chem.* **68**, 8790–8797 (2003)
- S. Herres, U. Flörke, G. Henkel, *Acta Crystallogr. C* **60**, o356–o360 (2004)
- A. Vlad, M. Avadanei, S. Shova, M. Cazacu, M.F. Zaltariov, *Polyhedron* **146**, 129–135 (2018)
- S.I. Gorelsky, L. Basumallick, J. Vura-Weis, R. Sarangi, K.O. Hodgson, B. Hedman, K. Fujisawa, E.I. Solomon, *Inorg. Chem.* **44**, 4947–4960 (2005)
- R.M. Silverstein, F.X. Webster, D.J. Kiemle, *Spectrometric Identification of Organic Compounds*, 7th Edition, ed. by D. Brennan, (New York, 2005)
- D. Filip, M. Asandulesa, D. Macocinschi, M. Aflori, S. Vlad, *J. Mater. Sci.* **51**, 8516–8528 (2016)
- C. Hamciuc, E. Hamciuc, T.V. Bubulac, S. Vlad, M. Asandulesa, A.W. Grabczyk, *Polym. Test* **52**, 94–103 (2016)

**Publisher’s Note** Springer Nature remains neutral with regard to jurisdictional claims in published maps and institutional affiliations.